Resolution dependence of petrophysical parameters derived from X-ray tomography of chalk

D. Müter, H. O. Sørensen, D. Jha, R. Harti, K. N. Dalby, H. Suhonen, R. Feidenhans'l, F. Engstrøm, and S. L. S. Stipp

Citation: Applied Physics Letters **105**, 043108 (2014); doi: 10.1063/1.4891965
View online: http://dx.doi.org/10.1063/1.4891965
View Table of Contents: http://scitation.aip.org/content/aip/journal/apl/105/4?ver=pdfcov
Published by the AIP Publishing

Resolution dependence of petrophysical parameters derived from X-ray tomography of chalk

D. Müter,[1] H. O. Sørensen,[1] D. Jha,[1] R. Harti,[1] K. N. Dalby,[1] H. Suhonen,[2] R. Feidenhans'l,[3] F. Engstrøm,[4] and S. L. S. Stipp[1]
[1]*Nano-Science Center, Department of Chemistry, University of Copenhagen, Universitetsparken 5, 2100 Copenhagen Ø, Denmark*
[2]*European Synchrotron Research Facility, Grenoble, France*
[3]*Nano-Science Center, Niels Bohr Institute, University of Copenhagen, Universitetsparken 5, 2100 Copenhagen Ø, Denmark*
[4]*Mærsk Oil and Gas A/S, Copenhagen K, Denmark*

(Received 20 May 2014; accepted 21 July 2014; published online 30 July 2014)

X-ray computed tomography data from chalk drill cuttings were taken over a series of voxel dimensions, ranging from 320 to 25 nm. From these data sets, standard petrophysical parameters (porosity, surface area, and permeability) were derived and we examined the effect of the voxel dimension (i.e., image resolution) on these properties. We found that for the higher voxel dimensions, they are severely over or underestimated, whereas for 50 and 25 nm voxel dimension, the resulting values (5%–30% porosity, 0.2–2 m^2/g specific surface area, and 0.06–0.34 mD permeability) are within the expected range for this type of rock. We compared our results to macroscopic measurements and in the case of surface area, also to measurements using the Brunauer-Emmett-Teller (BET) method and found that independent of the degree of compaction, the results from tomography amount to about 30% of the BET method. Finally, we concluded that at 25 nm voxel dimension, the essential features of the nanoscopic pore network in chalk are captured but better resolution is still needed to derive surface area. © *2014 AIP Publishing LLC*.
[http://dx.doi.org/10.1063/1.4891965]

Many hydrocarbon reservoirs in the North Sea Basin are hosted in chalk, which is a biogenic, nanoporous carbonate rock, often classified as limestone. Chalk also plays an important role as aquifers for groundwater in the countries that border the North Sea. The primary petrophysical parameters, e.g., porosity, surface area, and permeability, control how much oil can be produced, which has economic consequences and they affect the degree of contamination and the effectiveness of remediation in chalk aquifers, thus impacting the environment. Chalk porosity ranges widely from ~5% to 50%, but generally the connectivity of the pores is poor and pore throats are narrow so permeability is often very low, from 0.04 to 0.65 mD.[1–3] Chalk's pore network structure arises from its genesis, i.e., how it was formed, and its diagenesis, the processes that converted the initial calcareous mud into rock.

Chalk is formed from the remains of coccolithophorids, a group of algae species that create calcite, $CaCO_3$, shields to cover their one cell.[4,5] These shields, called coccoliths, are composed of 20–60 single, nanoscale crystals arranged radially. During diagenesis, compaction squeezes some of the water from the calcareous mud, fragmenting the coccoliths, but in contrast to nonbiogenic calcite, chalk retains most of its micro and nanostructure, even over geological time.[6,7] Because of the small size of the particles, the pores are also in the nanometer to micrometer range.

Macroscopic analysis delivers averaged values for the petrophysical parameters, but it is impossible to study the individual pores. Synchrotron based X-ray computed tomography (CT), also called X-ray micro- or nanotomography (XMT, XNT), can provide the resolution necessary for visualizing the pore networks in chalk. Segmenting the tomographic data into the solid and void phases makes it possible to determine the characteristic parameters such as porosity and surface area. To achieve the highest possible resolution, the samples must be less than a millimeter in diameter. It might sound preposterous to claim that the values found for individual, micrometer scale samples could be of direct significance for predicting the macro- or kilometer scale properties of rocks or reservoirs, but previous studies[8,9] have indicated that porosity and permeability correlate well over a range of length scales. However, to make this claim more robust, much more evidence is needed about how the individual parameters scale as resolution changes over several orders of magnitude.

In this work, our aim was to bridge the nano- to micrometer scale range, by analyzing a set of tomography data that were taken at the same X-ray source, on the same samples, over a range of resolution where voxel (volume pixel) dimension was systematically changed in steps from 320 nm to as little as 25 nm. By comparing the parameters derived from tomography with surface area derived using the Brunauer-Emmett-Teller method (BET)[10] and measurements made with traditional, macroscopic techniques, our purpose was to determine what resolution would be needed to derive parameters only from small particles that would represent the determining features of the pore network in very fine grained porous media.

Figure 1 shows chalk particles taken from drill cuttings (sample A: UK2 #16, sample B: UK2/2 #72, and sample C: UK2/2 #70) from a borehole in the Hod field (North Sea Basin). The samples were ~500 μm in diameter (Figure 2).

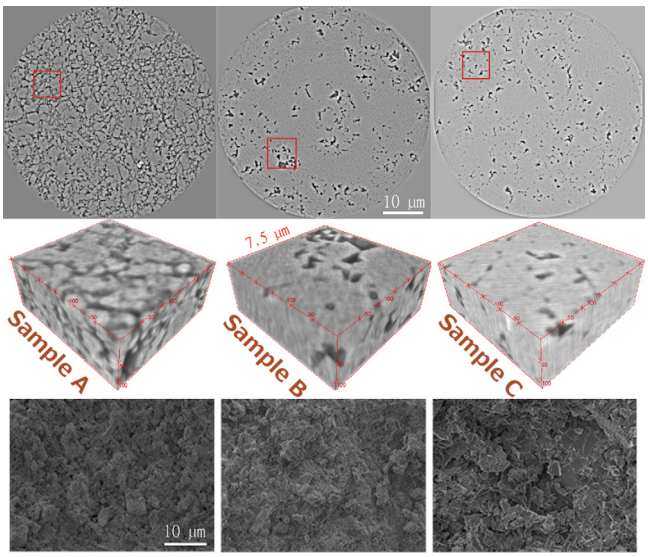

FIG. 1. Ring artifact corrected, single slices (top row) and 3D subvolumes (middle row) from the tomography data recorded at a voxel dimension of 25 nm for the samples examined in this work, labeled A, B and C, as well as SEM images (bottom row) showing their characteristic texture. The red squares in the top row mark the upper face of the 3D subvolumes. Dark regions represent pores.

Tomography data were collected at the ID22 beamline (29.49 keV) at the European Synchrotron Research Facility (ESRF), Grenoble, France. The beamline setup[11,12] allows data to be recorded at several levels of resolution. We acquired images with voxel dimensions of 320, 100, 50, and 25 nm, by using a conical beam and adjusting the distance between the sample and the detector.[22] For every distance, the sample was rotated 360°, while 1999 radiographs were collected with an exposure time of 0.5 s. The low resolution data sets were reconstructed using regular filtered back projection from just one distance, whereas four distances were used for the 100, 50, and 25 nm voxel dimensions using the holotomography reconstruction method.[23] The actual optical resolution, i.e., the distance at which two objects can be distinguished, is usually a factor of up to 6 lower than the voxel dimension. Two factors limit resolution: the X-ray focus size and the detector spread function. Both lead to a convolution with a Gaussian function. In addition, uncertainty about the sample rotation center can introduce artifacts into the reconstructed data. Thus, the best resolution achievable for our data was ~150 nm. The same or higher resolution is also possible with a scanning electron microscopy (SEM, Figure 1) combined with focused ion beam milling (FIB)[13] but in contrast to tomography, FIB-SEM destroys the sample. This makes time dependent investigations impossible, such as observing fluid flow or changes in pore geometry as a function of chemical reaction, but it can give very high resolution chemical composition.

The obvious difference between the three samples shown in Figure 1 is that samples B and C are highly compacted, whereas sample A is more porous. All samples consist almost exclusively of calcite, although we have seen other minerals, e.g., barite, in some of the samples (not included here[14]). Figure 2 shows data from samples A and B at the four voxel dimensions. At the lowest resolution (320 nm voxel dimension and ~1.9 μm optical resolution), the fine features are blurred and pore network details are poorly reproduced. Increasing the resolution, i.e., decreasing voxel dimension, naturally leads to better results. As voxel dimension decreases to 50 or 25 nm, individual rhombohedral calcite crystals become visible, such as are also observed in the SEM images (Fig. 1). However, at this high resolution, ring artifacts can occur, i.e., circular variations in the gray intensity (e.g., in sample C in the 3D subvolume in Fig. 1), which stem from imperfect correction for, e.g., inhomogeneous detector response and variations in the intensity profile of the incoming beam. These ring artifacts are not taken into account when reconstructing the sample density from the X-ray radiographs, which can pose a problem for segmenting the data into solid and void phases, introducing errors into the subsequently derived petrophysical parameters.[15]

The center of the concentric rings artifacts fluctuated throughout the volume by less than 1% so we could use an adaptive ring artifact suppression method to compensate for them, avoiding loss of resolution. The details of this algorithm are presented elsewhere.[15] Subsequently, the data were filtered and segmented, using our own approach,[16] which gave the results presented in Figure 3. Our dual filtering uses Unsharp Masking to increase the edge sharpness in the image, with subsequent median filtering to remove noise. Segmentation itself is then performed using traditional Otsu thresholding.[17] The visual quality of the resulting binarized images is convincingly improved.

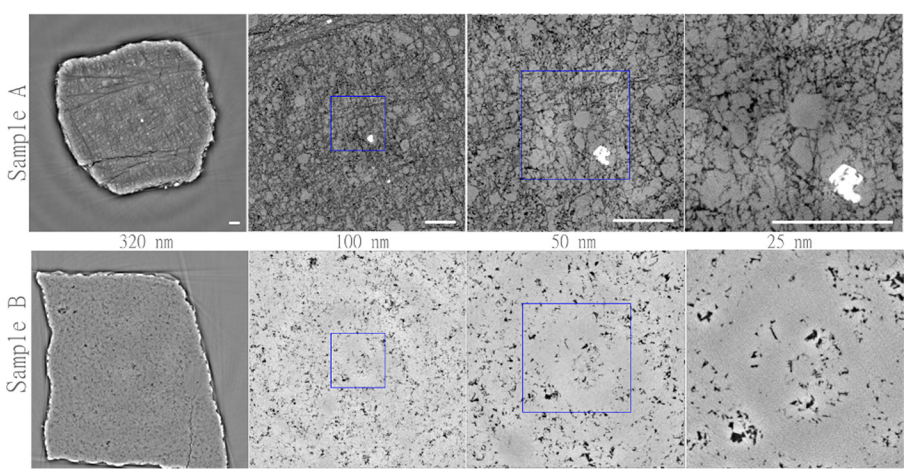

FIG. 2. Slices from the tomography data taken for samples A and B at four levels of resolution, where voxel dimension ranges from 320 to 25 nm. The white scale bar represents 20 μm in all images. The blue square in the 100 and 50 nm voxel dimension images marks the position of the 25 nm images. Dark regions represent pores and fractures. The images with voxel dimensions 100, 50, and 25 nm have been corrected for ring artefacts.[15] At the 320 nm voxel dimensions, alternating bright and dark rims around the sample can be seen. These stem from X-ray refraction at the sample surface.

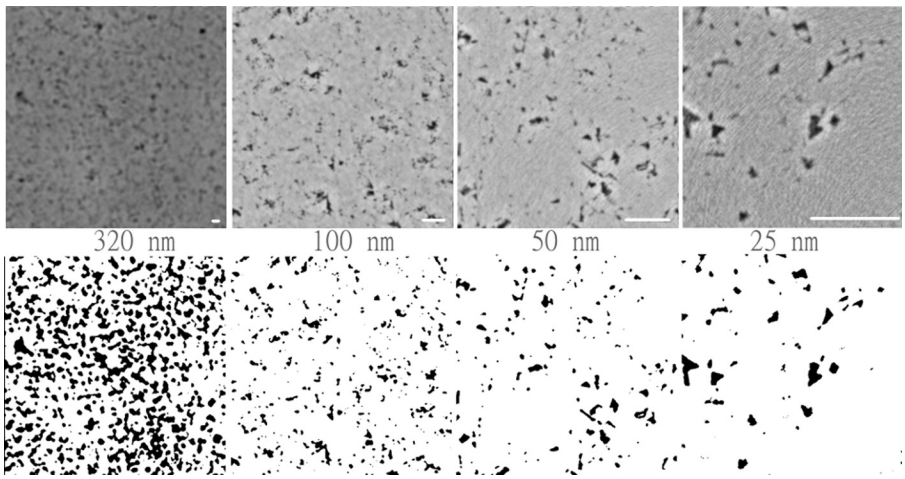

FIG. 3. Original and segmented slices of the tomography data for sample B at four zoom levels. Remnants of the ring artifacts can still be seen in the 25 nm voxel dimension image but these were removed before segmentation. The white scale bar represents 5 μm in all images. Dark regions represent pores.

Once the data were effectively segmented, the porosity can be easily extracted from the segmented volume image, as the ratio of number of void voxels (black in Figure 3) to the total number of voxels. In the simplest approach to calculate surface area, one would simply sum the number of voxel faces shared between void and solid and multiply by the square of the voxel dimension. However, this would represent a brick-like material, which would be quite unrealistic for natural materials. Pore throats, which we know are there and we can see, would be under represented. Therefore, we use the isosurface, a polygonal surface approximation, produced by the well known Marching Cubes algorithm.[18]

In our case, we construct the isosurface solely for the purpose of deriving a more realistic estimate for the surface area, or for comparison, the specific surface area, $\bar{A}$, which is defined as the surface area per gram of solid: $\bar{A} = A/(V(1-\varphi)\rho)$, where A represents the isosurface area, V is the volume of the tomography data (number of voxels $\times$ voxel volume), φ is the porosity, and ρ is the specific density. For ρ, we assume that the solid has a density of $\rho = 2.71\,\mathrm{g/cm^3}$ (calcite). This is supported by X-ray diffraction and chemical analysis, which identified less than 7% (sample B) to be other material and the X-ray attenuation factor from the tomograms, i.e., the gray intensity in Figures 1–3, which is fairly constant within each data set. Quartz and amorphous silica are the most abundant secondary phases and because of their very similar specific density ($\rho = 2.65\,\mathrm{g/cm^3}$), they would not change the density significantly.

A simple approach to extract absolute permeability, k, is provided by the Kozeny equation:[19] $k = \varphi^3/(2A^2)$, where φ denotes porosity and A is the surface area per bulk volume. The equation in this form,[20] however, assumes flow through capillary bundles or pipes, which is of course a very simplified view of the pore network in chalk.

In Figure 3, representative slices of the tomography data for sample B are shown for the four levels of resolution. For the 320 nm slice, blurring around the particle edges shows that resolution is too low, leading to low quality segmentation. With decreasing voxel size, visual quality of the original and the segmented data improves. At highest resolution, even individual calcite crystals and pore boundaries can be identified by their rhombohedral form. Calculating porosity and specific surface area from each of the segmented images leads to Figure 4. We have studied the dependence of porosity and surface area on the analyzed volume and found that a volume of 2×10^8 voxels is representative. Accordingly, the analyzed volume for all data sets is larger than this value.

Porosity derived from the low resolution data is severely overestimated (Fig. 4). It decreases rapidly with decreasing voxel size and is constant when determined from the two highest resolution datasets. The effect in sample A is more pronounced because the porosity is higher. As we approach the absolute limit of the resolution in the imaging setup, it is expected that porosity would not change anymore between 50 and 25 nm voxel dimensions. Specific surface area is severely underestimated from low resolution data for all

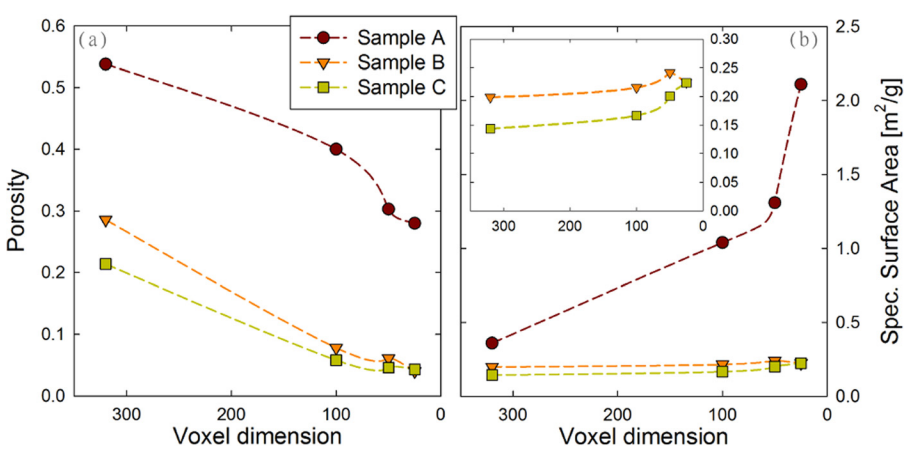

FIG. 4. Calculated porosity (a) and specific surface area (b) as a function of the voxel dimension for the three samples. Samples B and C are the compacted chalk; sample A is more porous.

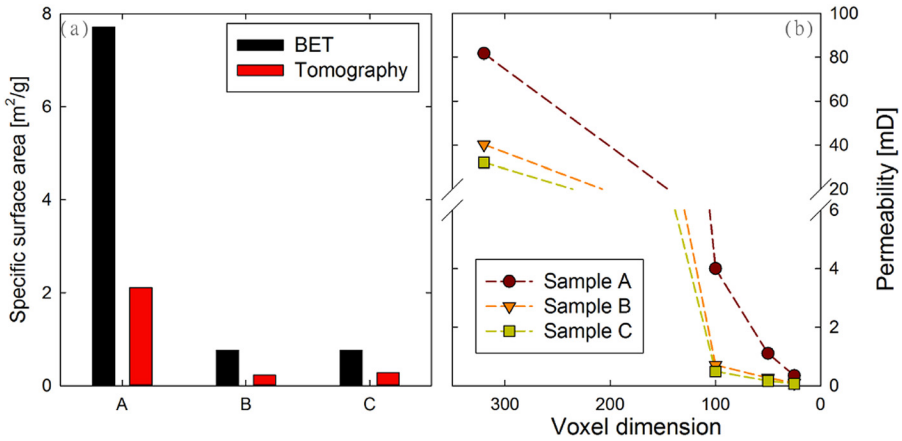

FIG. 5. Specific surface area from BET analysis and tomography images (a) and dependence of the permeability calculated from the specific surface area and porosity (Fig. 4) on the voxel dimension (b).

samples, but the increase in surface area estimate between the 50 nm and 25 nm voxel data is still quite significant, indicating that still higher resolution is needed to fully resolve the surface features. This is logical because smaller particles contribute proportionally more to surface area.

To assess the quality of the tomographic data independently, we can compare our results for porosity to macroscopic measurements on core plugs (tomographic/core data): sample B 4.0%/5.2% and sample C 4.3%/7.1%. Although the samples for the tomograms were about two orders of magnitude smaller, the values derived from tomography show good agreement with the core plug data. For sample A, macroscopic data were estimated based on burial depth from core log data. Accordingly, the deviation is somewhat larger: 28.0% (tomogram) and 14.2% (macroscopic data).

For surface area, we have to rely on literature values for North Sea Basin chalk. In contrast to porosity, specific surface area does not vary dramatically with burial depth, ranging from ~0.9 to 3.8 m^2/g.[1–3] The results for sample A at 25 nm voxel dimension fall into the expected range, indicating that this resolution is high enough to produce data that capture the essential features of the samples. For samples B and C, porosity and surface area are lower than the literature range but these samples were particularly well consolidated.

BET surface area analysis provides another point for comparison. BET[10] uses nonreactive gas adsorption to measure the internal surface area of a sample. The gas, in our case, nitrogen, is assumed to adsorb as a monolayer. In the adsorption isotherm, the shift to coverage beyond a monolayer is observable so the gas volume required to reach saturation can be converted to surface area using the dimension of the N_2 molecule.

In Figure 5(a), we have plotted the results from the highest resolution tomography data with the BET surface area results. The BET results are a factor of ~3.5 higher than the data derived from tomograms, which indicates that more surface area could be resolved if higher resolution were available. It is interesting though that the relative difference between the BET and tomography values is nearly the same for all samples (i.e., tomography values are ~30% of the BET values) and thus independent of porosity. This demonstrates that although samples B and C are more consolidated, the same relative amount of additional surface exists at a scale that is still not accessible with current, state-of-the-art tomography.

The inaccessible surface area can be explained by the difference in the size of the probe used in the two approaches. In BET analysis, the N_2 molecule is ~3 Å in diameter, whereas optical resolution is 150 nm for the 25 nm voxel dimension images. Clearly, a significant proportion of small pores are not counted in the surface area derived from tomography. However, for applying these results in oil production or soil and aquifer remediation, we can safely assume that a considerable portion of the additional surface area measured by BET is not accessible to the fluids of interest.

Using the Kozeny equation and the porosity and surface area from Figure 4, we determined the permeability. Figure 5(b) shows its dependence on voxel dimension.

In comparison with literature values from macroscopic measurements for the matrix permeability of North Sea chalk (0.01–20 mD, Ref. 1), our values for the lower resolution images are definitively too high. This is not surprising because the pore volume is clearly over determined. For data derived from the highest resolution images, permeability is in the same order of magnitude as in the macroscopic measurements on core plugs leading to quite good agreement (tomographic/macroscopic): sample A: 0.340 mD/0.065 mD, sample B: 0.09 mD/0.01 mD, and sample C: 0.06 mD/0.01 mD.

The obvious reason for the remaining small discrepancy is the missing of surface area. Because surface area is squared in the Kozeny equation, error naturally increases and one should keep in mind that the Kozeny equation is based on an idealized picture of the pore system, namely, parallel tubes. Nevertheless, Figure 5(b) shows that the Kozeny equation can provide meaningful values for permeability from tomographic data, if the resolution is high enough.

To summarize, X-ray tomography data collected on the same sample over a range of voxel dimensions provide an opportunity to assess the resolution needed for obtaining meaningful petrophysical parameters from chalk drill cuttings. After removing the ring artifacts, filtering, and segmenting, we can determine porosity and surface area using the Marching Cubes algorithm and these data improve in their match with macroscopic data as the voxel dimension decreases in the images used to collect the data. As expected, higher resolution captures a more realistic representation of porosity and surface area. Comparison of porosity and permeability with macroscopic measurements from the same samples shows reasonable to good agreement for the data

from the 25 nm voxel dimension images. Comparison of surface area derived from BET analysis shows significant underestimation, which can be attributed to the difference in the size of the "probe" used to measure with.

Thus, for applications in the fields of hydrogeology, groundwater remediation, and oil production, we conclude that a voxel dimension of 25 nm, or more precisely 150 nm optical resolution, should serve as an *upper boundary* for tomographic data on chalk. A foreseeable further increase in resolution, i.e., decrease of voxel dimension, as a result of improved technology, namely, a technique called ptychographic X-ray tomography[21] will probably close the gap between tomography image derived data and the BET results.

The research leading to these results has received funding from the People Programme (Marie Curie Actions) of the European Union's Seventh Framework Programme FP7/2007-2013/ under REA Grant Agreement No. 297921. We thank S. Pedersen for his help and the beamline scientists at the ID22 beamline at ESRF (European Synchrotron Research Facility) for their technical support. Funding was provided by the Danish Advanced Technology Foundation and Maersk Oil and Gas A/S through the P^3 project. Danscatt provided support for travel and accommodation at ESRF.

[1]M. A. Anderson, *Petroleum Research in North Sea Chalk* (RF-Rogaland Research, 1995).
[2]D. A. Belova, A. Johnsson, N. Bovet, L. Z. Lakshtanov, and S. L. S. Stipp, Chem. Geol. **291**, 217 (2012).
[3]M. L. Hjuler and I. L. Fabricius, J. Petrol. Sci. Eng. **68**, 151 (2009).
[4]Z. Balogh, C. S. Pedersen, L. L. Skovbjerg, T. Hassenkam, E. Johnson, K. Bechgaard, L. G. Benning, and S. L. S. Stipp, Geochim. Cosmochim. A **73**, A82 (2009).
[5]K. Henriksen, S. L. S. Stipp, J. R. Young, and P. R. Bown, Am. Mineral. **88**, 2040–2044 (2003).
[6]C. S. Pedersen, A. Johnsson, J. W. Nielsen, L. Z. Lakshtanov, K. Bechgaard, I. Damager, and S. L. S. Stipp, Geochim. Cosmochim. A **73**, A1007 (2009).
[7]L. N. Schultz, K. Dideriksen, L. Lakshtanov, S. S. Hakim, D. Müter, F. Hausser, and S. L. S. Stipp, Cryst. Growth Des. **14**, 552–558 (2014).
[8]J. Mortensen, F. Engstrøm, and I. Lind, SPE Reservoir Eval. Eng. **1**, 245 (1998).
[9]S. Kynde, F. Engstrøm, T. H. Jensen, R. Feidenhans'l, and S. L. S. Stipp, "Using X-ray microtomography to obtain a 3D representation of the pore space in North Sea chalk" (unpublished).
[10]S. Brunauer, P. H. Emmett, and E. Teller, J. Am. Chem. Soc. **60**, 309 (1938).
[11]T. Weitkamp, C. Raven, and A. Snigirev, Proc. SPIE **3772**, 311 (1999).
[12]A. Koch, C. Raven, P. Spanne, and A. Snigirev, J. Opt. Soc. Am. **15**, 1940 (1998).
[13]H. Yoon and T. A. Dewers, Geophys. Res. Lett. **40**, 4294, doi:10.1002/grl.50803 (2013).
[14]H. O. Sørensen, S. S. Hakim, S. Pedersen, B. C. Christiansen, Z. I. Balogh, C. P. Hem, I. S. Pasarin, S. Schmidt, U. L. Olsen, J. Oddershede *et al.*, Can. Mineral. **50**, 501–509 (2012).
[15]D. Jha, H. O. Sørensen, S. Dobberschütz, R. Feidenhans'l, and S. L. S. Stipp, "Adaptive ring artifact suppression for tomography applications," Appl. Phys. Lett. (submitted).
[16]D. Müter, S. Pedersen, H. O. Sørensen, R. Feidenhans'l, and S. L. S. Stipp, Comput. Geosci. **49**, 131 (2012).
[17]N. Otsu, IEEE Trans. Syst. Man Cybern. **9**, 62–66 (1979).
[18]W. E. Lorensen and H. E. Cline, in *SIGGRAPH'87 Proceedings of the 14th Annual Conference on Computer Graphics and Interactive Techniques* (1987), p. 163.
[19]J. Kozeny, Sitzungsber. Akad. Wiss., Wien **136**(2a), 271 (1927).
[20]A. Y. Dandekar, *Petroleum Reservoir Rock and Fluid Properties* (CRC Press, 2006), p. 52.
[21]H. N. Chapman, Nature **467**, 409 (2010).
[22]J. Vilanova, J. Laurencin, P. Cloetens, P. Bleuet, G. Delette, H. Suhonen, and F. Usseglio-Viretta, J. Power Sources **243**, 841–849 (2013).
[23]P. Cloetens, W. Ludwig, J. Baruchel, D. van Dyck, J. van Landuyt, J. P. Guigay, and M. Schlencker, Appl. Phys Lett. **75**, 2912 (1999).